Earthq Eng & Eng Vib (2014) 13: 555-568 **DOI**: 10.1007/s11803-014-0262-9

Simplified dynamic analysis to evaluate liquefaction-induced lateral deformation of earth slopes: a computational fluid dynamics approach

Yaser Jafarian[1†], Ali Ghorbani[2†] and Omid Ahmadi[2‡]

1. *International Institute of Earthquake Engineering and Seismology, P.O. Box 19395-3913, Tehran, Iran*
2. *Faculty of Engineering, University of Guilan, Rasht, Iran*

Abstract: Lateral deformation of liquefiable soil is a cause of much damage during earthquakes, reportedly more than other forms of liquefaction-induced ground failures. Researchers have presented studies in which the liquefied soil is considered as viscous fluid. In this manner, the liquefied soil behaves as non-Newtonian fluid, whose viscosity decreases as the shear strain rate increases. The current study incorporates computational fluid dynamics to propose a simplified dynamic analysis for the liquefaction-induced lateral deformation of earth slopes. The numerical procedure involves a quasi-linear elastic model for small to moderate strains and a Bingham fluid model for large strain states during liquefaction. An iterative procedure is considered to estimate the strain-compatible shear stiffness of soil. The post-liquefaction residual strength of soil is considered as the initial Bingham viscosity. Performance of the numerical procedure is examined by using the results of centrifuge model and shaking table tests together with some field observations of lateral ground deformation. The results demonstrate that the proposed procedure predicts the time history of lateral ground deformation with a reasonable degree of precision.

Keywords: liquefaction; lateral ground deformation; simplified dynamic analysis; computational fluid dynamics

1 Introduction

Earthquake-induced liquefaction has caused significant damage to civil engineering structures such as lifeline facilities and foundations. Lateral ground deformation is the most devastating consequence of soil liquefaction that occurs in free-face and gentle slopes. Reports of ground failure during several recent earthquakes such as the Kobe 1995, Chi-Chi 1999, Kocaeli 1999, and Nisqually 2001 reminds the engineers that this type of deformation should be considered in the design of foundations. Recent advances in seismic design based on performance criteria and some new concepts such as L.C.C. (Life Cycle Cost) have encouraged the development of methodologies for the precise estimation of lateral ground displacements.

The current methodologies for estimation of liquefaction-induced lateral displacement are classified into three major categories: empirical relationships, analytical procedures, and numerical approaches. Empirical relationships are based on field observations and have the most applications in practice. The early empirical equations of lateral spreading (Hamada *et al*., 1986) considered geometric attributes of the ground while more recent equations (Youd *et al*., 2002) also accounted for the seismological parameters and engineering properties of soil. Bartlett and Youd (1992) compiled a database of liquefaction-induced ground displacement involving 448 entries from seven earthquakes. They used multi-linear regression and presented two separate empirical relationships for free-face and gently sloping ground conditions. These models were subsequently modified by Youd *et al*. (2002). In recent years, several researchers (e.g., Baziar and Ghorbani, 2005; Javadi *et al*., 2006) obtained more precise equations through advanced soft computing tools. Since the empirical models were developed using field case histories, scattered predictions are to be expected due to the limitations of such observations. Nevertheless, these empirical procedures have merit since they have been developed based on direct field measurements.

Newmark (1965)'s sliding block procedure was the first analytical method thatis applicable for estimation of lateral ground displacement. Several subsequent

Correspondence to: Yaser Jafarian, International Institute of Earthquake Engineering and Seismology, P.O. Box 19395-3913, Tehran, Iran
Tel: +98-21-22831116 Ex. 454
E-mail: yjafarianm@iiees.ac.ir
†Assistance Professor;‡ Graduate Student

Supported by: International Institute of Earthquake Engineering and Seismology (IIEES) under Grant No. AM-7/507-6 723-545
Received May 6, 2013; **Accepted** Feburary 13, 2014

procedures were developed to modify the sliding block method (e.g., Rathje and Bray, 1999; Rathje and Antonakos, 2011). Towhata *et al*. (1992) developed an analytical model based on the minimum potential energy principle and observations from shaking table experiments.

Researchers have also implemented advanced constitutive models for numerical evaluation of liquefaction-induced lateral spreading. Based upon the presumed mechanical behavior of the liquefied soil, several numerical schemes have been proposed by researchers. Elgamal *et al*. (2002) employed a multi-surface plasticity framework to simulate cyclic mobility and the consequent lateral spreading, while Dafalias and Popov (1975) dealt with the framework of the critical state.

In addition the conventional frameworks of constitutive modeling for soil liquefaction, liquefied soil can be simulated as stiffness-reduced solid or viscous fluid (Naili, 2006). This view point has evolved into an interesting perspective for numerical estimation of lateral spreading. Yasuda *et al*. (1992) proposed a simple static finite element analysis in which a predefined soil stiffness switches to a decreased post-liquefaction stiffness to simulate permanent lateral spreading. Aydan (1995) proposed an adaptive finite element mesh by considering liquefied soil as viscoelastic material. Uzouka *et al*. (1998) assumed liquefied soils as Bingham fluid and proposed a numerical method based on fluid dynamics to predict lateral deformation of sand. They estimated the deformations produced by the flow liquefaction, which basically occurs when the shear stresses required for equilibrium are larger than the residual (or steady state) shear strength.

The current study incorporates the concept of fluid dynamics to estimate liquefaction-induced lateral deformations of earth slopes subjected to cyclic liquefaction or flow failure. The proposed numerical procedure treats the liquefiable soil as linear elastic material with varying strain-adaptive stiffness before the yield stress and as Bingham fluid during failure. Degradation of shear modulus, which is an outcome of significant generation of pore water pressure and liquefaction onset, is defined through an iterative procedure. Residual strength of the soil is considered as a reasonable post-liquefaction parameter for the Bingham model to simulate the large strain state of liquefied soil. Some well-known experimental models like geotechnical centrifuge and shaking table tests are simulated to examine the capability of the proposed procedure. Some case histories of liquefaction-induced lateral deformation are then simulated and the results are compared with the observed displacements as well as predictions of the previously proposed models. Results of the numerical simulations are employed for a multi-linear regression analysis and the resulting equation is compared with some well-known empirical relationships proposed by other researchers.

2 Bingham fluid, flow failure, and cyclic mobility

A Bingham fluid is a viscoplastic material that maintains significant rigidity at low stresses but flows as a viscous fluid at high stress. The Bingham model requires fewer calibration parameters compared with advanced constitutive model sand hence might be advantageous for the assessment of soil lateral deformation. Uzouka *et al*. (1998) modeled the liquefied soil as a Bingham fluid; its shear stress-strain rate relation is expressed as:

$$\tau = \mu\dot{\gamma} + \tau_r \tag{1}$$

where τ is the total shear stress, μ is the viscosity, τ_r is the yield stress which is equal to the minimum (or residual) shear strength of soil, and $\dot{\gamma}$ is the second invariant of the shear strain rate tensor:

$$\dot{\gamma} = \sqrt{(\frac{1}{2})\dot{\boldsymbol{e}}_{ij}\dot{\boldsymbol{e}}_{ij}} \tag{2}$$

where $\dot{\boldsymbol{e}}_{ij}$ is the deviatoric strain rate tensor as given by:

$$\dot{\boldsymbol{e}}_{ij} = \frac{1}{2}[\frac{\partial \dot{u}_i}{\partial x_j} + \frac{\partial \dot{u}_j}{\partial x_i}] \tag{3}$$

To treat the liquefied soil as an incompressible Bingham fluid, Uzouka *et al*. (1998) expressed the Bingham viscosity by the equivalent Newtonian viscosity:

$$\mu' = \mu + \frac{\tau_r}{2\dot{\gamma}} \tag{4}$$

The residual shear strength of soil, considered as the minimum undrained strength in Eqs. (1) and (4), is the threshold of yielding occurrence. Uzouka *et al*. (1998) simulated an experiment conducted by Hamada *et al*. (1986) in which a soil container was initially liquefied and then gradually inclined to produce flow deformation. The main feature of this experiment was the triggering of lateral deformation without dynamic excitation. For the numerical implementation of the Bingham fluid model, Uzouka *et al*. (1998) considered the post-liquefaction stress state of soil and predicted lateral deformation of the liquefied sloping ground due to the self-weight. This type of deformation is known as flow liquefaction or flow failure, which occurs once the unbalanced shear stresses exceed the residual shear strength. In reality, however, lateral deformation of the sloping grounds might be produced during the cyclic loading while the unbalanced stresses are smaller than the residual shear strength of soil. This type of lateral ground deformation takes place as a result of cyclic mobility. Thus, it seems essential to capture this type of ground deformation through computational fluid dynamics.

3 Proposed numerical procedure

To simulate the procedure of liquefaction-induced

lateral deformation, soil is assumed to behave like viscoplastic materials. The Bingham materials have a certain value of yield stress and behave the same as a solid when the applied stresses are lower than the yield stress. It then deforms like a viscous fluid once the yield stress is surpassed. Saturated sands under cyclic loading tolerate a variety of stress excitations and maybe liquefied. Thus, it is important for the implementation of the model to compute the actual imparted stresses to determine whether yielding occurs. The incremental elastic stress model incorporating the Bingham model has been employed in the current study to determine the stress state during earthquake excitation and resulting lateral deformation.

Figure 1 summarizes the procedure of the proposed CFD-based numerical analysis through a flowchart. Accordingly, the first step begins by determination of some model parameters such as the maximum shear modulus and the residual shear strength of the soil under consideration. Two types of analyses are subsequently categorized as flow liquefaction and cyclic mobility. Flow liquefaction deformation is produced when the soil tolerates the driving in-situ shear stresses larger than the residual strength of the soil. Lateral deformations can also occur during the cyclic mobility for which the in-situ shear stresses are less than the residual shear strength. The right side of the flowchart, which shows how the flow failure type of deformations is estimated, is the same as the numerical procedure of Uzouka *et al*. (1998).

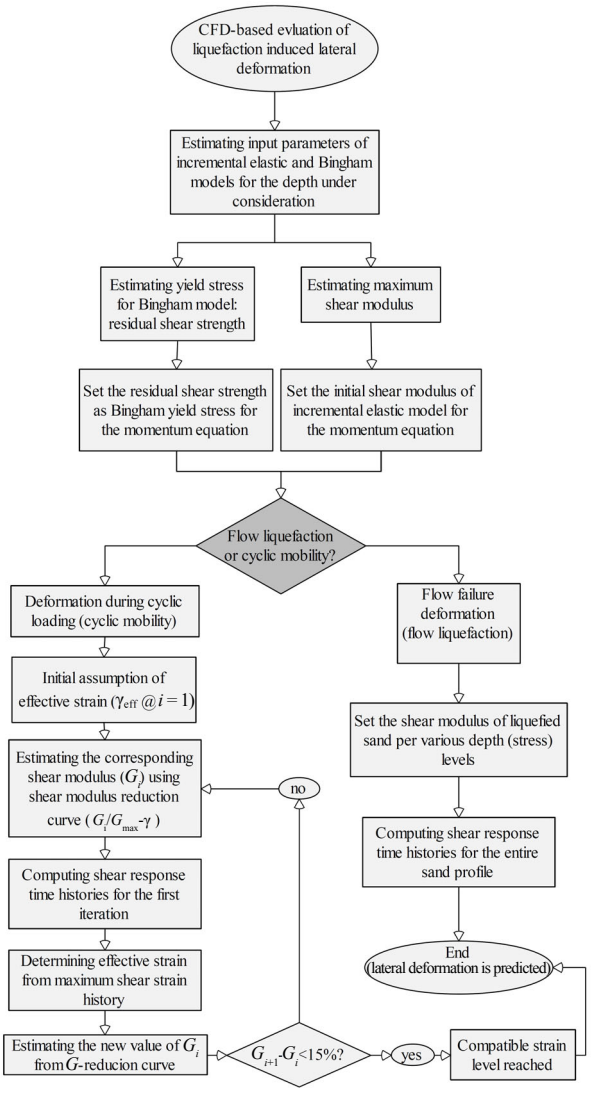

Fig. 1 Procedure of the CFD-based numerical analysis

The proposed numerical scheme incorporates soil parameters in both solid and liquefied phases through a simplified numerical procedure. It contains both small and large strain states of soil and conjunction of these states which is defined through the shear modulus-reduction curve of the soil. The maximum shear modulus and residual shear strength of the soil are considered to be representative of small and large strain conditions, respectively, as described in the following subsections.

3.1 Governing equation

Viscoplasticity describes the rate-dependent inelastic response of solids; meaning that deformation of the material depends on the rate at which loads are applied. The inelastic response is plastic deformation and implies that the material undergoes irrecoverable permanent deformations once a prescribed shear stress level is surpassed. In contrast to Hookean elastic solids, the state of stress for a Newtonian viscous fluid is (Brethour, 2003):

$$\boldsymbol{T} = 2\mu\dot{\boldsymbol{E}} \tag{5}$$

where μ is the viscosity coefficient, $\dot{\boldsymbol{E}}$ is the strain rate tensor, and $\boldsymbol{T}$ is the Cauchy stress tensor. Figure 2 illustrates a schematic simplification of viscoplastic materials.

A viscoplastic model predicts a corresponding rise in elastic stress that is linearly proportional to the strain. If further strain is imposed to the extent where the elastic stress exceeds the yield stress, the material yields and begins to flow as a viscous fluid with an equivalent viscosity. The incremental elastic stress model was recently implemented into FLOW-3D to predict highly nonlinear responses through an incremental elastic procedure. The developed code utilizes a fixed-mesh Eularian approach to compute the elastic stresses. For an element of fluid, the basic equation of the incremental elastic model description is:

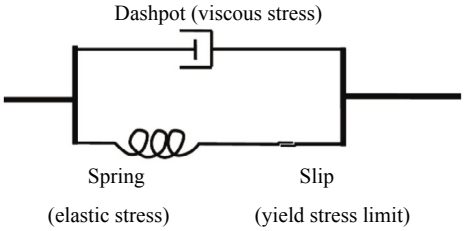

Fig. 2 Pictorial view of viscoplastic model

$$\boldsymbol{\tau}_E(\xi,t)=\int_{-\infty}^{t}2G\dot{\boldsymbol{E}}(\xi,t')\mathrm{d}t' \tag{6}$$

where $\boldsymbol{\tau}_E$ is the stress tensor and ξ is the material coordinate which rotates and translates with the deforming material.

The Misescriterion is employed to predict the yielding condition:

$$\Pi_{\tau_E}=\frac{Y^2}{3} \tag{7}$$

where Π_{τ_E} is the second invariant of the elastic stress tensor and Y is a yield stress limit; a material parameter. If there is a region in material where the elastic stress exceeds the yield criterion, the elastic stress is relaxed by:

$$\boldsymbol{\tau}_E^{\,*}=\sqrt{\frac{2Y^2}{3\Pi_{\tau_E}}}\boldsymbol{\tau}_E \tag{8}$$

where $\boldsymbol{\tau}_E^{\,*}$ is the yield-limited elastic stress tensor. The resulting momentum equation, which includes the elastic stress tensor $\boldsymbol{\tau}_E^{\,*}$, is obtained as:

$$\frac{\partial \boldsymbol{u}}{\partial t}+\boldsymbol{u}\cdot\nabla\boldsymbol{u}=-\frac{1}{\rho}\nabla P+\frac{1}{\rho}\left\{\nabla\cdot\left[\mu\left(\nabla\boldsymbol{u}+(\nabla\boldsymbol{u})^{\mathrm{T}}\right)\right]+\boldsymbol{F}_{\mathrm{b}}+\nabla\cdot\boldsymbol{\tau}_E^{*}\right\} \tag{9}$$

where ρ is the fluid density, P is the pressure, μ is the dynamic viscosity, and F_{b} represents the body forces (per unit volume) acting on the fluid.

3.2 Model parameters

3.2.1 Shear modulus

In the previous sections, the incremental elastic stress model was explained to consider small strain conditions and the method of estimating elastic stress distribution was demonstrated. For the proposed procedure, the strain-compatible shear modulus of the soil has to be estimated. It has been well recognized that liquefiable soils behave in a highly nonlinear manner, and this is manifested in the shear modulus, which significantly reduces with shear strain under cyclic loading (Ishihara, 1996). Figure 3 shows the backbone and corresponding shear modulus reduction curves of a typical liquefiable soil.

The shear modulus is high at low strain amplitudes but it decreases as the strain amplitude increases. The backbone's slope at the origin represents the maximum shear modulus, G_0 or $G_{\max}$ (also known as small-strain shear modulus). Nonlinear or degradable behavior is observed at the greater cyclic strain amplitudes where the shear modulus ratio (G_{sec}/G_0) considerably declines to low values.

The description of the stiffness of a soil element requires consideration of both G_0 and variation of the shear modulus ratio with shear strain (G-reduction curve) (Kramer, 1996). To define the strain-compatible shear modulus of an incremental elastic model, an equivalent linear approximation was employed. An iterative procedure was implemented to find a shear modulus value which is compatible with the shear strain amplitude of the soil layer.

The iterative procedure includes the following steps:

- An initial estimate of G is made for the selected depth of the layer. It is usually recommended to choose initial values at low strain levels.
- The estimated value of G is used to compute the ground response, including time histories of shear strain. The input acceleration or shear stress time history is defined in the FLOW-3D program to perform this step.
- The effective shear strain of the selected depth is determined from the maximum shear strain in the computed shear strain time history. It is common to obtain the strain level of seismic loading in terms of an effective strain, which has been found to vary between 50% to 70% of the maximum shear strain. Here, the effective strain in each step has been predicted by this equation, according to Seed *et al*. (1975):

$$\gamma_{\mathrm{eff}}=0.65\gamma_{\max} \tag{10}$$

where $\gamma_{\max}$ is the maximum shear strain at the depth under consideration. From this effective shear strain, a new value of G is adopted for the next iteration from the predefined G-reduction curve. As indicated in Fig.1, these steps are repeated until the difference between the values of computed shear modulus in two successive

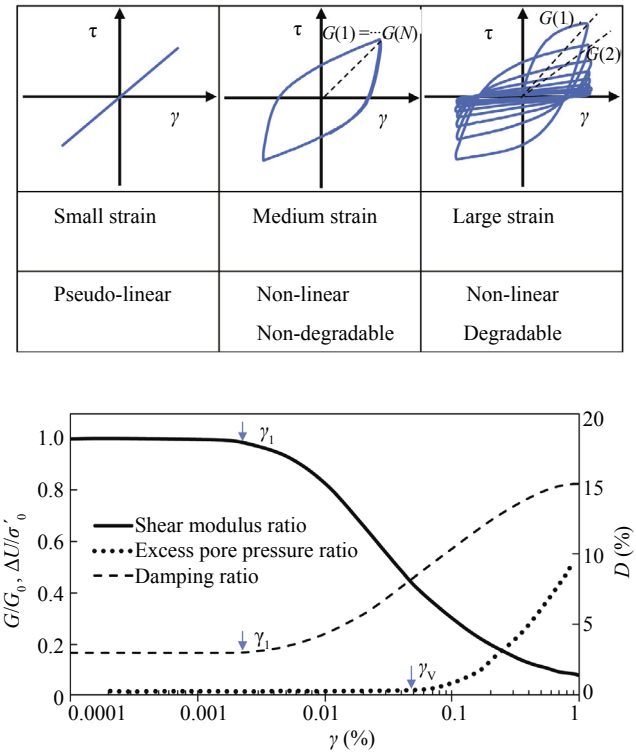

Fig. 3 Backbone curve showing typical variation of G_{sec} with shear strain

iterations falls below 10%.

It is also required to determine the maximum shear modulus of the soil layer at the desired depth to use in the equivalent linear approximation. The maximum shear modulus of soil can be obtained from laboratory tests such as a resonant column, bender element, and precisely-instrumented cyclic triaxial test. The shear modulus at small strains is strongly dependent on the effective confining stress and void ratio of the soil. Several researchers have proposed empirical relationships for various sands in the general form of (Kokusho, 1980):

$$G_0 = A \cdot F(e) \cdot (\sigma_0')^n \tag{11}$$

where A and n are calibration parameters, $F(e)$ is a simple function of soil void ratio and σ_0' is the mean effective stress. When the results of field tests such as blow counts of standard penetration tests (SPT) are available, dependable correlations are employed to estimate relative density and the corresponding void ratio of the soil (Cubrinovski and Ishihara, 1999; Seed, 1987). Use of such correlations is unavoidable, especially when estimating soil properties of field case histories.

3.2.2 Residual strength of liquefied soil

In this study, the residual strength of liquefied soil, S_{ur}, is considered as the yield stress, which mimics the transition between the elastic solid and the viscous fluid conditions. The residual strength, in fact, is the strength of the soil tolerating large shear strain such as liquefaction. In the terminology of soil liquefaction studies, this parameter is also referred to as post-liquefaction or steady-state strength. Figure 4 shows the stress-strain behavior of two specimens of Toyoura sand subjected to monotonic and cyclic-monotonic undrained shearing at a relative density of 16% and initial effective confining pressure of 0.1 MPa. Loose sands with a high initial confining pressure commonly exhibit contractive behavior throughout the shearing. This results in dramatic increase of excess pore water pressure, which leads to significant strain softening just after the peak point, as depicted in Fig. 4. As seen in this figure, over the range of moderate to large strains, the stress-strain curve for the monotonic loading is almost coincident with those obtained for the cyclic-monotonic loading (Ishihara, 1996). In fact, the residual strength of sands is expected to be irrespective of the prior cyclic stress history.

There are currently two methods for estimating the residual strength of soil deposits: (1) back analysis of the flow failed case histories and correlation of the residual strength with in-situ resistance such as standard penetration test blow counts (SPT) (Seed and Harder, 1990), and (2): laboratory-based procedures (Baziar and Dobry, 1995). Use of SPT-based residual strength for numerical evaluation of lateral deformation maybe desirable for case studies. Several researchers have presented empirical recommendations for S_{ur}. Idriss and Boulanger (2008) presented two recommendations to predict the residual strength, S_{ur}, and the residual strength normalized to the initial effective overburden stress, S_{ur} / σ_{v0}'. Seed (2010) reviewed Idriss and Boulanger (2008)'s report and indicated considerable over-estimation of S_{ur} for some case histories that were previously reported in Seed (1987). Finally, Seed (2010) recommended the dashed line shown in Fig. 5 to estimate the residual strength in terms of the SPT blow counts corrected for the effects of overburden pressure, hammer energy, and fines content ($(N_1)_{60cs}$). The current study employs Seed (2010)'s recommendation to estimate residual strengths of the simulated problems. However, these recommendations (Seed, 2010; Idriss and Boulanger, 2008) are being coincide for the corrected SPT blow counts of around 10 (see Fig. 5), which is the value of interest for the benchmark case histories in the current study. The numerical methodology has been verified using the results from two physical model tests and some field case histories.

4 Application to physical models and field case histories

The proposed numerical scheme was described in the preceding sections. This procedure is applied to some

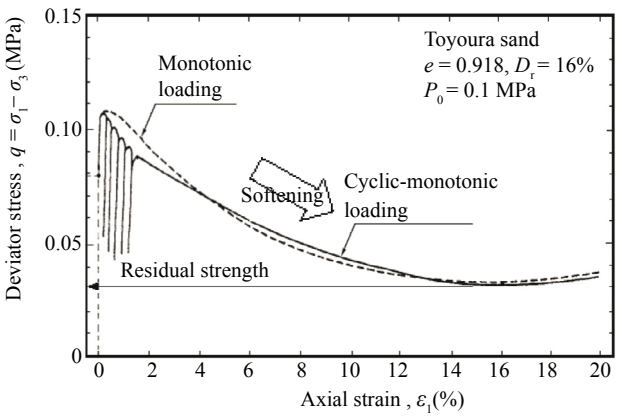

Fig. 4 Schematic idea of stress-strain behaviour of soil in triaxial compression test and residual strength of sand in large strain level (after Ishihara, 1996)

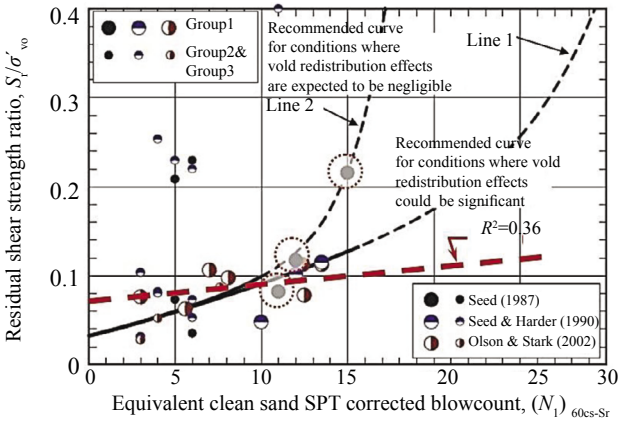

Fig. 5 Recommendations of Seed (2010) based on the interpretations of Idriss and Boulanger (2008)

benchmarks from previously conducted experimental works that simulated lateral soil deformations due to flow liquefaction and cyclic mobility. The following subsections aim to examine the applicability and capability of the proposed procedure for geotechnical centrifuge, shaking table, and actual earthquake conditions.

4.1 Centrifuge test simulation

Geotechnical centrifuge testing of soil is a useful means to investigate a wide range of geotechnical engineering problems. A centrifugal device rotates a model container around the central axis and the generated centrifugal force allows simulation of a field prototype with smaller model. The VELACS centrifuge model No. 2 was conducted by Dobry and Taboada to simulate a mildly inclined infinite slope with an effective inclination angel of about 4˚ for prototype scale. This is a fully referenced centrifuge test, which was employed by several numerical studies for verification purposes (VELACS Project).

The principle of geotechnical centrifuge testing is to maintain the stresses in the model at the same values as at homologous point in a prototype. A centrifuge acceleration of *N*g means that the unit weight of soil in the centrifuge container is *N* times greater than the unit weight at the 1 g condition, while the stresses in the test remains the same as in a full-scale situation. Table 1 shows the law of similitude for typical dynamic centrifuge tests (Towhata, 2008). Table 2 presents the basic soil properties of Nevada sand, which was used in the centrifuge experiment.

There are corrections which should be considered when the prototype results are estimated from the model results. For the VELACS model No. 2, Taboada (1995) corrected the total unit weight of the sand using a coefficient as follows:

$$\gamma_{\text{teff}} = c\gamma_{\text{t}} \tag{12}$$

where γ_{t} stands for the total unit weight of the soil in the prototype scale and the value of c = 1.294 was set by Taboada (1995) to obtain $\gamma_{\text{teff}} = 25.05$ kN/m^3 for model No. 2. Correction for in-situ shear stress results in an angle of slope inclination, α_{field}, equal to 4˚ (Taboada, 1995).

The centrifuge test was simulated using this numerical procedure implemented in FLOW-3D. To simulate the free surface condition at the top of the container, the specific boundary pressure with a zero *F* fraction ratio was utilized and a non-slip wall boundary was specified for the other boundaries (see Fig. 6(a)). In fluid dynamics, the non-slip condition for viscous fluids states that at a solid boundary, the fluid will have zero velocity relative to the boundary. A non-slip wall boundary was specified for the viscous fluid states at solid boundaries with zero relative velocity. A boundary with zero *F* fraction ratio was utilized to set the void into the domain. In FLOW-3D, for free-surface problems with hydrostatic boundaries, the top boundary is a void pressure boundary (i.e., fluid fraction = 0).

Determination of the input parameters for the implemented procedure such as Bingham viscosity and small-strain shear modulus was explained in the preceding sections (see Fig. 1). For the simulated centrifuge model, the equation proposed by Cubrinovski and Ishihara (1999) was employed to correlate relative density and SPT blow counts for the estimation of residual strength from the empirical graphs shown in Fig. 5.

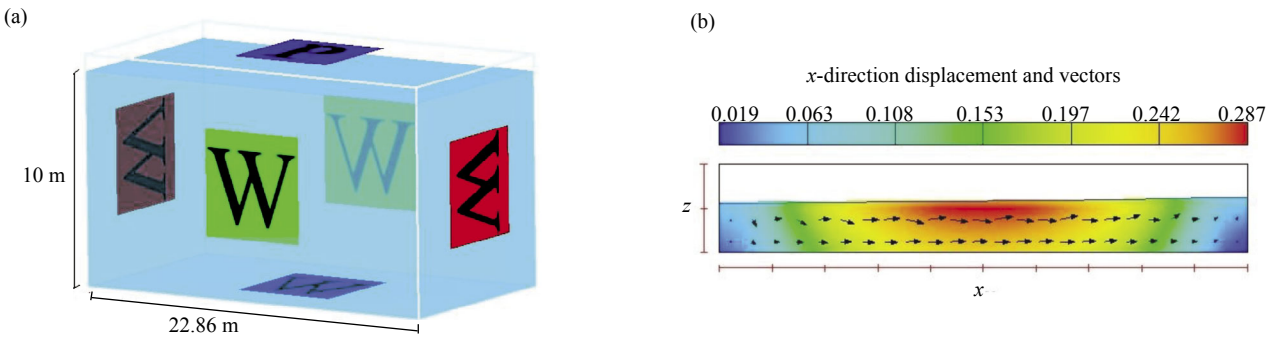

Fig. 6 (a) Boundary conditions of centrifuge model in 3D-Flow; (b) Contours and vectors of lateral ground deformation

Table 1 Similitude law in dynamic centrifuge model test (Towhata, 2008)

Parameters	Prototype	Model	Parameters	Prototype	Model
Size	*n*	1	Displacement	*n*	1
Mass density	1	1	Velocity	1	1
Gravity	1	*n*	Acceleration	1	*n*
Unit weight	1	*n*	Time	*n*	1
Stress	1	1	Strain	1	1

$$\frac{(N_1)_{60}}{D_r^2} = \frac{11.7}{(e_{max} - e_{min})^{1.7}} \quad (13)$$

For Nevada sand with D_r = 40% and the maximum and minimum void ratios cited in Table 2, the $(N_1)_{60}$ value of about ≈ 10 is obtained. Consequently, the residual strength can be easily derived from Fig. 5. Table 3 summarizes the values of the corrected penetration resistances ($(N_1)_{60}$ = 9.8, $(N_1)_{60cs}$= 11), fines content (= 7%), and the residual strength (= 7.5 kPa) of Nevada sand according to Seed (2010)'s recommendation. The quantities were determined in the middle of the soil layer as representative of the whole layer.

The Bingham viscosity can then be found by the following equation, which is switched once stresses surpass the yield stress (τ_r):

$$\mu' = \mu + \frac{\tau_r}{2\dot{\gamma}} = 695 + \frac{3750}{\dot{\gamma}} \quad (14)$$

where μ' is the equivalent Bingham viscosity (Pa·s), $\dot{\gamma}$ is the strain rate (1/s), and μ is the constant viscosity at a strain rate of zero. For the incremental elastic stress model, the small-strain shear modulus, G_0 must also be specified. As shown in Fig. 1, an iterative procedure was carried out to determine the strain-compatible shear modulus from the *G*-reduction curve. Various equations are found to obtain the maximum shear modulus of sands, as summarized in Table 4. As seen, the equations basically have the same functional form with different *A* coefficients and *n* exponents. In order to determine these calibration parameters for Nevada sand, curve fitting was applied on the results of the resonant column tests, which were conducted as part of the VELACS project. Accordingly, the calibration parameters, i.e., *A* and *n*, were found to be equal to 6500 and 0.5, respectively. Table 4 presents a comparison between the previous relationships and the estimated *A* and *n* values.

Table 2 Soil properties in the centrifuge model test

Soil	Density	D_r	e_{max}	e_{min}
Nevada sand	1962 kg/m^3	40%	0.887	0.511

Table 4 Constants in empirical equations on small strain modulus, after Ishihara (1996)

Reference	*A* (kPa)	*F*(*e*)	*n*
Hardin and Richart (1963)	7000	$\frac{(2.17-e)^2}{(1+e)}$	0.5
Iwasaki *et al*. (1987)	9000	$\frac{(2.17-e)^2}{(1+e)}$	0.38
Kokusho (1980)	8400	$\frac{(2.17-e)^2}{(1+e)}$	0.5
Based on resonant column tests on Nevada sand		$A \cdot F(e) = 7700$	0.5

An iterative operation was utilized by assuming an initial *G* at low strain levels and using the estimated *G* to compute the response including the time histories of shear strain for the depth of 0.7 m where LVDT3 was installed near the ground surface.

To determine the effective shear strain, Eq. (10) along with the *G*-reduction curve was repeatedly used to estimate new G^{i+1} for the next iteration. These steps are repeated until differences between the computed shear modulus in two successive iterations fall below a pre-determined value. Figure 7 shows the shear modulus reduction curve employed during the iteration procedure (WSDOT). The procedure was carried out for the different values of shear modulus obtained from Table 4. Figure 8 illustrates the trace of the iterative procedure for various estimations of initial shear modulus. They follow the predefined *G*-reduction curve of sand, as shown in Fig. 7. Accordingly, the iterative procedure yields the strain-compatible shear modulus; and thus, a more reasonable dynamic stress regime is achieved.

Figure 9 compares the predicted and measured time histories of lateral ground deformation at a depth of 0.7 m near the surface. The measured lateral displacement was recorded by LVDT3, which is the closest instrument to the ground surface. The predicted time histories were estimated based on the various values of initial (small-strain) shear modulus (see Table 4). This may be useful in examining the sensitivity of the modeling to the initial shear modulus estimate. Figure 9 confirms that the numerical modeling obtains reasonable performance since the measured time history of lateral deformation falls within the range of the predictions with various small-strain shear moduli.

The procedure proposed in this study addresses numerical dynamic analysis of liquefied layers through a simplified framework. Thus, for simplicity, some

Table 3 Estimation of residual strengths from various recommendations

$(N_1)_{60}$	*FC* (%)	$(N_1)_{60}$ – CS	Residual strength (kPa)
9.87	7	11	7.5

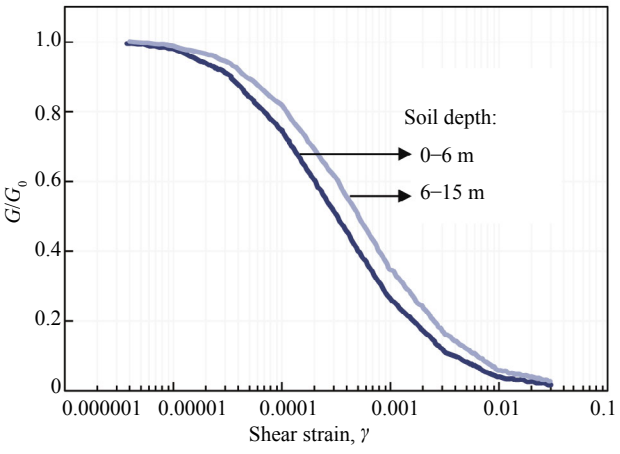

Fig. 7 Shear modulus reduction curve (EPRI, 1993)

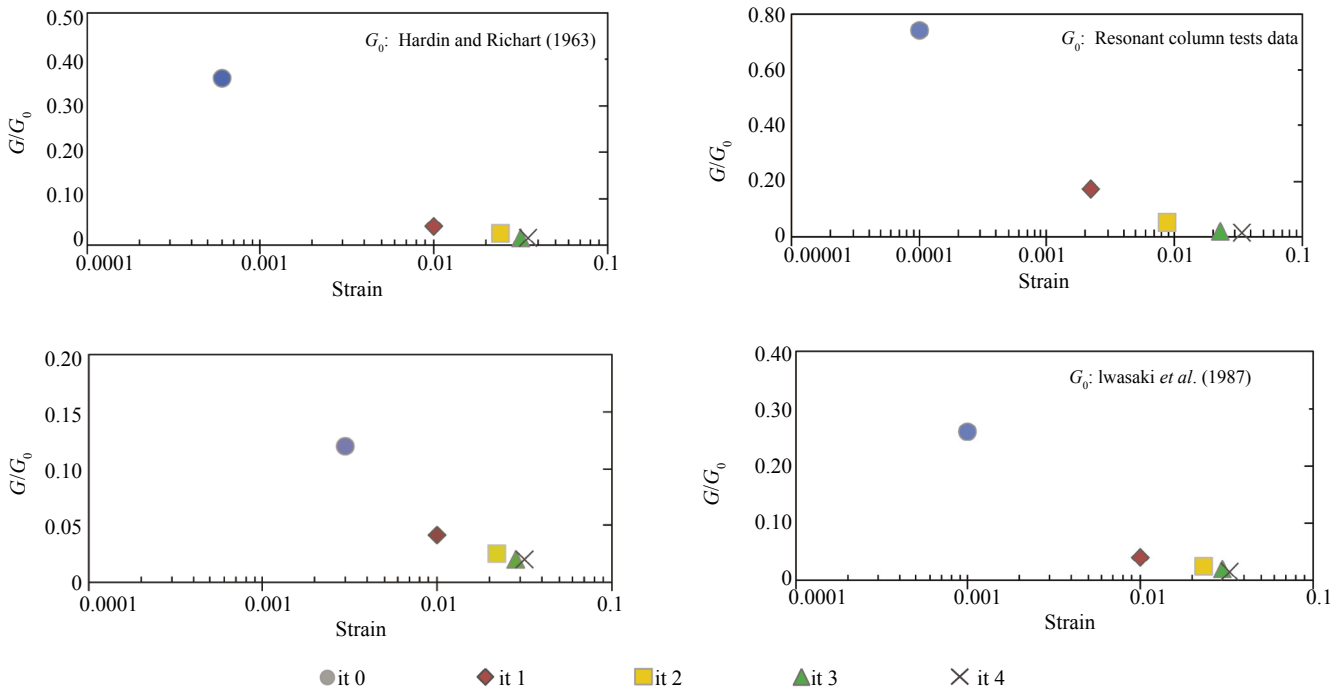

Fig. 8 Iteration analysis at the ground level of soil layers

primary mechanisms of soil liquefaction have to be indirectly considered. The dynamic curve of sand, i.e., *G*-reduction, is utilized in order to indirectly account for the physical aspects of liquefied sands. As shown in Fig. 3, stiffness degradation of sand due to the generation of excess pore water pressure occurs when the imparted shear strain surpasses the threshold volumetric strain. In other words, residual pore water pressure generates in sands once the imparted shear strain exceeds the threshold volumetric strain. It is aconsequence of the saturated sand tendency to the irrecoverable volumetric strain. Therefore, implementation of the *G*-reduction curve in the proposed procedure indirectly accounts for excess pore water pressure provided the imparted shear strain is larger than the threshold shear strain. Figure 8 illustrates that the imparted shear strain surpasses the shear strain of 0.01%, which is close to the volumetric shear strain threshold reported by Vucetic (1994).

4.2 Shaking table experiment

In this section, capability of the proposed model in simulation of 1 g shaking table test is examined. The numerical simulation was carried out on a 1 g shaking table test conducted by Hamada *et al.* (1986). The soil box was 3 m (length), 1m (width) and 0.3 m (height). It was vibrated in the lateral direction until liquefaction occurred, and then lifted using a jack to enforce the soil to ensure flow failure. During the experiment, the final shape of the free surface was continuously monitored and the time histories of the induced displacements were measured. Considering that lateral displacement was triggered once the slope inclination reached 2% (Hamada *et al.*, 1986), the minimum undrained strength (equivalent to the residual shear strength) was estimated as 54 by Naili (2006) for model scale according to the slope stresses equilibrium and the following equation:

$$\tau_{\min} = \gamma \cdot h \cdot \cos\theta \cdot \sin\theta \tag{15}$$

where γ and h are the saturated unit weight and the thickness of the liquefied soil layer, respectively, and θ is slope inclination. Contrary to the previously analyzed centrifuge experiment, which was simulating cyclic mobility during cyclic loading (the left branch of the flowchart in Fig. 1), the shaking table test simulates the flow type of failure or flow liquefaction, described in the right side of the flowchart shown in Fig. 1. For an initial relative density of 40% to 50%, the shear modulus of the liquefied sand is approximately 1% of its initial small-strain shear modulus (Olsen, 2008). Since the entire soil mass in the box was liquefied, the small-strain shear

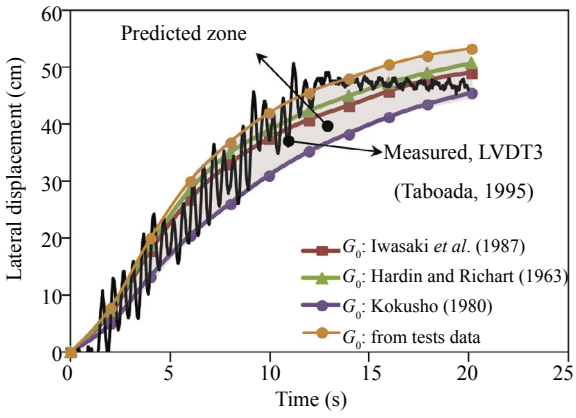

Fig. 9 Measured and predicted time histories of lateral ground deformation at depth = 0.7 m

modulus was estimated herein using Seed *et al*. (1984)'s correlation, cited in Table 5, and then multiplied by 1%.

In order to simulate the free surface condition at the container top, the specific pressure boundary with zero *F* fraction ratios was utilized and a non-slip wall boundary was specified for the other boundaries. The simulation was carried out for the prototype scale rather than the 1-g model because the employed correlation of shear modulus is more compatible to the actual effective stress levels. Since the stress level in the 1-g test is lower than in the prototype scale, the similitude law (e.g., Kokusho, 1980) has to be considered to represent the actual response. The similitude law recommended by Iai was employed in this study for numerical simulation of the experiment in the prototype scale. In simulating the prototype scale, a modification of the relative density of soil was considered using the applicable indices such as the brittleness index (Bishop *et al*., 1971). Figure 10 illustrates variations of the brittleness index versus relative density based on the results of ring shear tests (Vargas-Monge, 1998; Towhata, 2008). This is an experimental solution to achieve similitude in vulnerability of liquefied sand to flow and large deformation (Towhata, 2008) .

Figure 11 shows variations of soil surface velocity versus time up to only 3 s (for illustrative purposes); however, final stoppage of soil movement occurs at 12 s. As seen, soil velocity increases dramatically within 0.1 s to reach the maximum value (5 cm/s) and then declines rapidly up to 0.4 s. Thereafter, the liquefied soil tends for stoppage with a very small rate. The maximum value of the predicted soil velocity is 5 cm/s, which is in good agreement with the measured 7 cm/s maximum velocity of the soil surface (Hamada *et al*., 1986). The time history of the predicted lateral displacement was compared (see Fig. 12) with the measured displacement together with the curve predicted by Naili (2006). Naili (2006) simulated this shaking table tests using the SPH (Smoothed Particle Hydrodynamics) method. These results demonstrate the relative success of the current simulation compared with the SPH method and its reasonable agreement with the measured values.

4.3 Casehistory: Kocaeli (Izmit) earthquake

The 17 August 1999 Kocaeli-Turkey earthquake was an event with a moment magnitude of 7.4, and caused extensive liquefaction–induced ground displacements along the coast of Izmit Bay (Cetin *et al*., 2004). Cetin *et al*. (2004) reported the geological setting, ground motions, and observed liquefaction-induced lateral ground displacements of some sites. The results of these site investigations, including the results of standard penetration test (SPT), were used to predict the observed displacements through several empirical and semi-empirical procedures. These procedures involve two empirical models developed by Youd *et al*. (2002) and Hamada *et al*. (1986) and the semi-empirical

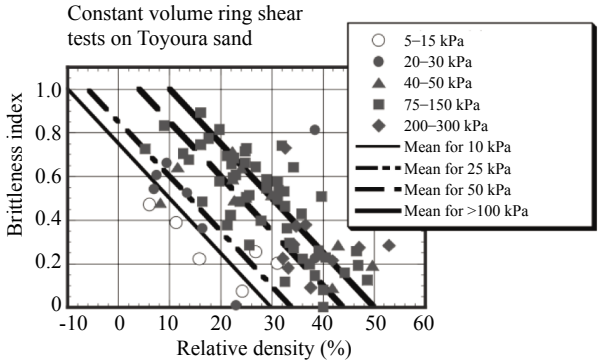

Fig. 10 Combination of relative density and effective stress level which keeps brittleness index constant (after Vargas-Monge, 1998; Towhata, 2008)

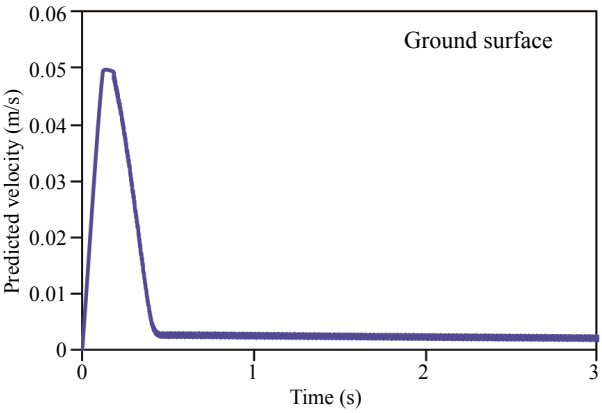

Fig. 11 Predicted velocity time histories of shaking table test

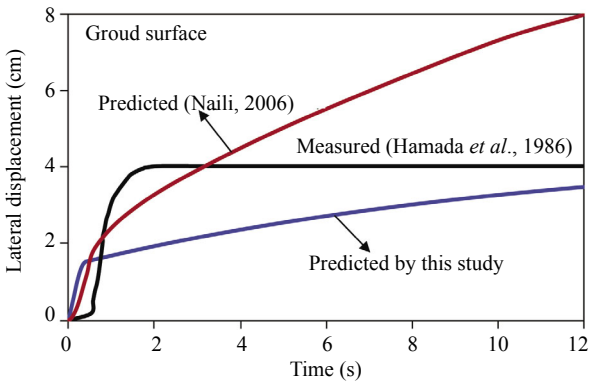

Fig. 12 Comparison between the simulated and measured values of lateral displacements proposed by Naili (2006)

Table 5 Soil properties and estimation of maximum shear modulus of shaking table experiment (Naili, 2006)

Case	D_r (%)	θ %	Unit weight (kN/m^3)	H (cm)	Correlation of maximum shear modulus (Seed, 1987)	Estimated G_0 (MPa)
EFM3	40	4.2	18	30	$G_0=220(K_2)_{max}(\sigma'_0)^n$ $(K_2)_{max}=20(N_1)_{60}^{(1/3)}$	15.88

model of Shomato *et al*. (1998). A comparison was then made between the observed and the predicted ground displacements. Figure 13 shows a site map of the Kocaeli case histories (Cetin *et al*., 2004).

The first step is to obtain suitable ground motion as the base ground motion in the numerical model. Cetin *et al*. (2004) estimated maximum ground accelerations of about 0.40 g for the Degirmendere Nose, Soccer Field, and Police Station sites. By considering this maximum acceleration and correcting it to use as base accelerations of the soil layer, the proposed acceleration time history is shown in Fig. 14. This seismic input motion was prepared with the acceleration time history recorded at the nearest strong ground motion station, i.e., the YPT Station (see Fig. 13). Similar to Cetin *et al*. (2004), a simplified linear scaling was done for the simulated liquefied soil layer. To account for the depth effect and produce the base ground motion, the depth reduction coefficient developed by Seed and Idriss (1971) was used instead of the deconvolution analysis, and the corrected input motion was simply produced (Fig. 14).

The case history analysis was carried out using a 3D model similar to the physical model tests. However, results of 3D and 2D analyses are equivalent for the case history analyses because out-of-plane spatial variations of the soil profile were ignored for simplicity. Simulations for the case history were performed by the thickness of the effective (liquefied) zone based on the reported boreholes and surface inclination of the site.

Using the Youd *et al*. (2002), Hamada *et al*. (1986), and Shomato *et al*. (1998) models, lateral ground displacements were estimated for several sites and borehole locations by Cetin *et al*. (2004). The reported values from the standard penetration test results were used in this study to evaluate the residual strength of the liquefied sub layers. As seen before, it is important to estimate the thickness of the liquefied layer for the numerical modeling and to define the residual shear strength. In their empirical model, Youd *et al*. (2002) proposed T_{15} as the best indicator of the liquefied layer for $6 \le M \le 8$ earthquakes. This parameter, i.e. T_{15}, is the cumulative thickness of the layers of saturated cohesion less sediments having $(N_1)_{60} \le 15$ up to a depth of 20 m. They found reasonable performance for this parameter without performing the liquefaction susceptibility analysis (Youd *et al*., 2002). Although T_{15} is not the actual cumulative thickness of the liquefied layers, it is directly estimated from the boreholes, which is useful in practice. Accordingly, T_{15} was considered as the coherent thickness of the soil layer in the numerical analyses, which is referred to as the liquefied layer hereafter. Table 6 presents the estimated parameters that were used in the numerical analyses of the three sites. In this table, G_0 is the maximum shear modulus of the liquefied layer, which was estimated using the correlation cited in Table 5, S_{ur} is the residual shear strength at the middle of the liquefied layer, W is the free face ratio, θ is the ground slope in percent, and H is the total-thickness (m) of the liquefied layers.

Cetin *et al*. (2004) compared the observed values of lateral deformation with those predicted by the models proposed by Youd *et al*. (2002), Hamada *et al*. (1986), and Shomato *et al*. (1998). Table 7 summarizes the parameters of these models.

Numerical modeling of these sites was also carried out using the proposed procedure and the estimated parameters are cited in Table 6. In Table 8, the results

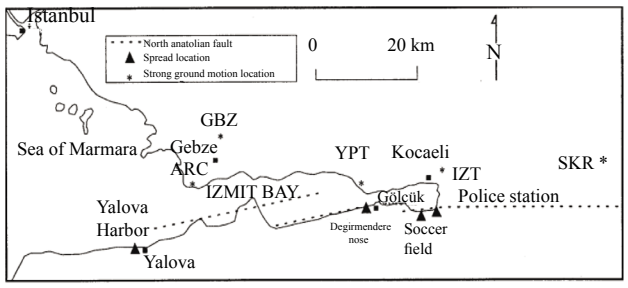

Fig. 13 Case history site map (after Cetin *et al*., 2004)

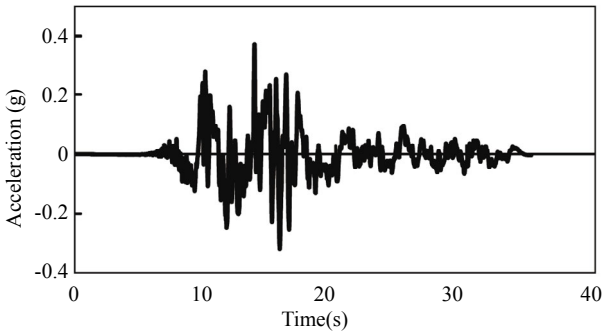

Fig. 14 Scaled acceleration time history of Yarimca (YPT) Station, used as base motion in numerical analysis

Table 6 Estimated parameters in the numerical analysis

Site	G_0 (MPa)	S_{ur} (kPa)	θ (%)	T_{15}/H (%)	W (%)
DN1	67	4.5	17	14.8	20
DN2	75	5	17	0	5
SF5	27	2	0	100	7
SF6	25	1	0	100	15
PS2	22	2.2	10	72.9	8
PS3	28	1.9	1	62.9	6
PS4	23	2.6	1	70	8

Table 7 Employed parameters in the referenced empirical models

Reference model	Used parameters of models
Hamada *et al*. (1986)	H = total thickness of liquefied layer θ = slope of the ground surface or the base of liquefied layer
Youd *et al*. (2002)	M = earthquake magnitude R = horizontal distance to nearest seismic source S = gradient of surface topography or ground slope W = free face ratio T_{15} = thickness of saturated layer with $(N_1)_{60} \le 15$ F15 = average fines content in T15 And D50
Shomato *et al.* (1998)	CSR (cyclic stress ratio) and residual shear strain

Table 8 Comparison of the predicted and the observed displacements in Kocaeli (Izmit) earthquake

Location	Observed displacement (cm)	Predicted displacement (cm)			
		Hamada (1986)	Youd *et al*. (2002)	Shomato *et al*. (1998)	Eq. (16) (this study)
DN1	90	440	120	97	163
DN2	0	440	0	3	0
SF5	30	0	74	12	25.7
SF6	120	0	240	49	142
PS2	240	310	300	72	180.2
PS3	10	120	180	10	13.6
PS4	90	98	60	4	11
Coefficient of determination (R^2)		0.0059	0.58	0.43	0.65
RMSE (cm)		223.1	85	76.6	47.4

of the simplified numerical analyses are compared with the observed values as well as predictions of the empirical models. Accordingly, the results of the simulations show a good agreement with the observed displacements in light of the coefficient of determination (R^2) and root of the mean squared error (RMSE). The resulting displacements cited in Table 8 were input into a multi variable regression (MVR) to determine a linear relationship between the magnitude of lateral displacements and the input parameters. Accordingly, the following equation has obtained to predict lateral deformation for the site:

$$D_{\mathrm{h}} = 51.68 - 0.19\times(0.01G_0) - 46.99\times S_{\mathrm{ur}} + 8.19\times W + 16.3\times\theta + 0.62\times\left(\frac{T_{15}}{H}\right) \quad (16)$$

where D_{h} is the lateral ground deformation in cm, G_0 is the small-strain shear modulus in kPa, S_{ur} is residual shear strength in kPa, W is the free-face ratio in percent, θ is the ground slope in percent, T_{15} is the thickness of saturated layer with $(N_1)_{60} \le 15$, and H is the total thickness of the liquefied layer. It is clear that has to be zero for the cases with zero values.

5 Summary and conclusions

This study incorporates the concept of fluid dynamics to estimate liquefaction-induced lateral deformations of earth slopes during cyclic liquefaction and flow failure. The proposed numerical procedure treats the liquefiable soil as a linear elastic material with varying strain-adaptive stiffness before the yield stress and as Bingham fluid during failure. An iterative procedure is introduced to estimate the adaptive dynamic shear stiffness of soil during the small strain state. The residual strength of the soil is considered as a reasonable post-liquefaction parameter for the Bingham model to simulate the large strain state of liquefied soil. The numerical procedure was implemented in FLOW-3D to model a single sloping layer of liquefiable soil.

Some well-documented physical models like geotechnical centrifuge and shaking table tests were simulated to examine the capability of the proposed procedure. Acentrifuge test simulating a mildly inclined infinite slope was numerically modeled. Determination of the input parameters of the implemented procedure such as Bingham viscosity and small strain shear modulus was explained. The results confirm that the

numerical model obtains reasonable performance since the measured time history of lateral deformation at the ground surface falls within the range of the predictions obtained by various small-strain shear moduli**.** The numerical simulation was also carried out for a 1 g shaking table test, conducted to simulate deformations that resulted in flow liquefaction. The time history of the predicted lateral displacement was compared with the measured displacement together with the curve predicted by previous researchers. These results demonstrate the relative success of the simulation compared with previous studies and its reasonable agreement with the measured values. The proposed model was applied to the simulation of a case history of lateral spreading during the Kocaeli 1999 earthquake using reported acceleration time history and tests data. The results from site investigations, including the results of standard penetration test (SPT), were used to predict the observed displacements through several empirical and semi-empirical procedures. Numerical modeling of these sites was also carried out using the proposed procedure and the estimated input parameters. The results of the proposed simplified numerical analyses have been tabulated for eight sites together with the observed values and predictions of the available empirical models. Accordingly, the results of the simulations show good agreement with the observed displacements in terms of the coefficient of determination (R^2) and root of mean squared error (RMSE).

For numerical estimation of lateral ground displacement, the current study has developed a simplified procedure with fewer parameters than the commonly used plasticity constitutive models. Although applicability and accuracy of the proposed procedure were verified for physical model tests and field conditions, it may produce imprecise results in some unexamined conditions such as layered soil profiles. Further study is required for modeling of layered soil profiles as well as homogeneous soil layers with the liquefied/nonliquefied sublayers.

Notation

A	Calibration parameters for initial shear modulus
CFD	Computational fluid dynamics
D_h	Lateral ground deformation
D_r	Relative density
E	Strain tensor
$\dot{E}$	Strain rate tensor
$\dot{e}_{ij}$	Components of the strain rate tensor
e_{max}	Maximum void ratio
e_{min}	Minimum void ratio
$F(e)$	Calibration parameter for initial shear modulus according to void ratio
G	Shear modulus
G_0 or G_{max}	Maximum shear modulus
G_{sec}	Secant shear modulus
H	Parameter that define the geometry
M	Earthquake magnitude
n	Calibration parameter for initial shear modulus
$(N_1)_{60}$	Corrected SPT count number
S_{ur}	Residua lundrained shear strength
T	Cauchy stress tensor
T_{15}	Cumulative thickness of sublayers with $(N_1)_{60} \le 15$
u	Local velocity vector
W	Parameter that define the geometry
Y	Yield stress limit
α_{field}	Angle of slope inclination
$\dot{\gamma}$	Shear strain rate
γ_{eff}	Effective shear strain
γ_{max}	Maximum shear strain
ε	Material coordinate
θ	Parameter that define the geometry
μ	Viscosity coefficient
μ'	Equivalent Bingham viscosity
Π_{τ_E}	Second invariant of the elastic stress tensor
ρ	Density
σ'_0	Mean effective stress
σ'_{v0}	Initial effective consolidation stress
τ	Total shear stress
τ_E	Stress tensor
τ_E^*	Yield limited elastic stress tensor
τ_{min}	Minimum undrained strength
τ_r	Yield stress

References

Aydan O (1995), "Mechanical and Numerical Modeling of Lateral Spreading of Liquefied Soil," *Proc.1st Int Conf on Earth-Geo Eng*, Tokyo, 881–886.

Bartlett SF and Youd TL (1992), "Empirical Analysis of Horizontal Ground Displacement Generated by Liquefaction-induced Lateral Spreads," *Technical Report No. NCEER-91-0021*, National Center for Earthquake Engineering Research. State University of New York at Buffalo, NY.

Baziar MH and Dobry R (1995), "Residual Strength and Large-deformation Potential of Loose Siltysands," *Journal of Geotechnical Engineering*, **121**(12): 896–906.

Baziar MH and Ghorbani A (2005), "Evaluation of Lateral Spreading Using Artificial Neural Networks," *J Soil Dyn Earthquake Eng*, **25**: 1–9.

Brethour JM (2003), "Incremental Elastic Stress Model," *Flow Science*, *Inc* FSI–03–TN64.

Brown JD (1971), "A New Ring Shear Apparatus and its Application to the Measurement of Residual Strength," *Geotech*., **21**(4): 273–328.

Cetin KO, Youd TL, Seed RB, Bray JD, Stewart JP, Durgunoglu HT, Lettis W and Yilmaz MT (2004), "Liquefaction-induced Lateral Spreading at Izmit Bay During the Kocaeli (Izmit)-Turkey Earthquake," *Journal of Geotechnical and Geoenvironmental Engineering*, **130**(12): 1300–1313.

Curbrinovski M and Ishihara K (1999), "Empirical Correlation between SPT N-value and Relative Density for Sandy Soils," *Soils and Found*, **39**(5): 61–72.

Dafalias YF and Popov EP (1975), "A Model of Nonlinearly Hardening Materials of Complex loadings," *Acta Mechanica*, **21**(3): 173–92.

Electrical Power Research Institute (EPRI) (1993), *Guidelines for Site Specific Ground Motions*, Palo Alto, CA, Electrical Power Research Institute, November-TR-102293.

Elgamal A, Yang Z and Parra E (2002), "Computational Modeling of Cyclic Mobility and Post-liquefaction Site Response," *Journal of Soil Dynamics and Earthquake Engineering*, **22**: 259–271.

Flow-3D (2008), *User Manual*, Version 9.3, Flow Science, Inc.

Hamada M, Yasuda S, Isoyama R and Emoto K (1986), "Study on Lquefaction-induced Permanent Ground Displacements," *Association for Development of Earthquake Prediction*, Japan.

Hardin BO and Richart FE (1963), "Elastic Wave Velocities in Granular Soils," *Journal of Soil mechanics and Foundations*, ASCE, **89**(SM1): 33–65.

Idriss IM and Boulanger RW (2008), "Soil Liquefaction during Earthquakes," *Monograph Series*, *No. MNO-12*, Earthquake Engineering Research Institute.

Ishihara, K (1996), *Soil Behaviour in Earthquake Geotechnics*, Oxford University Press Inc.

Iwasaki T, Tatsuoka F, Tokida K, and Yasuda S (1987), "A Practical Method for Assessing Soil Liquefaction Potential Based on Case Studies in Various Sites in Japan," *Proceedings of the 2nd International Conference on Microzonation for Safter Construction-Research and Application*, **2**: 85–96.

Javadi AA, Rezania M and Mousavi Nezhad M (2006), "Evaluation of Liquefaction Induced Lateral Displacements Using Genetic Programming," *J Computers and Geotechnics*, **33**: 222–233.

Kokusho T (1980), "Cyclic Triaxial Test of Dynamic Soil Properties for Wide Strain Range," *Soils and Foundations*, **20**: 45–60.

Kramer SL (1996), *Geotechnical Earthquake Engineering*, Prentice-Hall, Inc.

Naili M (2006), "Analysis of Liquefaction Induced Lateral Ground Displacement Using Smoothed Particle Hydrodynamics," *Ph.D Dissertation*, University of Tsukba, pp. 135.

Newmark NM (1965), "Effects of Earthquakes on Dams and Embankments," *Geotechnique*, **15**(2): 139–160.

Olsen PA (2008), "Shear Modulus Degradation of Liquefying Sand: Quantification and Modeling," *M.Sc. Thesis*, Brigham Young University.

Olsen SM and Stark TD (2002), "Liquefied Strength Ratio from Liquefaction Flow Case Histories," *Canadian Geotechnical Journal*, **39**: 629–647.

Rathje EM and Antonakos G (2011), "A Unified Model for Predicting Earthquake-induced Sliding Displacements of Rigid and Flexible Slopes," *Soil Dynamics and Earthquake Engineering*, **122**(12): 51–60.

Rathje EM and Bray JD (1999), "An Examination of Simplified Earthquake–induced Displacement Procedures for Earth Structures," *Canadian Geotechnical Journal*, **36**(1): 72–87.

Seed HB (1987), "Design Problems in Soil Liquefaction," *Journal of Geotechnical Engineering*, ASCE, **113**(8): 827–845.

Seed HB and Idriss IM (1971), "Simplified Procedure for Evaluating Soil Liquefaction Potential," *J Soil Mech Found Div*, ASCE, **97**(SM8): 1249–1274.

Seed HB, Mori K and Chan CK (1975), "Influence of Seismic History on the Liquefaction Characteristics of Sands," *Report EERC* 75–25, Earthquake Engineering Research Center, University of California, Berkeley, 1975-08, 33 pages.

Seed HB, Wong RT, Idriss IM and Tokimatsu K (1984), "Moduli and Damping Factors for Dynamic Analysis of Cohesionless Soils," Earthquake Engineering Research Center, *Report No. UCB/EERC–84/14*.

Seed RB (2010), "Technical Review and Comments: 2008 EERI Monograph, Soil Liquefaction during Earthquakes," *Geotechnical Report*.

Seed RB and Harder LF (1990), "SPT-based Analysis of Cyclic Pore Pressure Generation and Undrained Residual Strength," *Proceedings of Memorial Symposium for H. Bolton Seed*, J Michael Duncan ed., BiTech Publishers, Vancouver, B. C., Canada, 2, pp. 351–376.

Shomato Y, Zhang J and Tokimatsu K (1998), "New Charts for Predicting Large Residual Post-liquefaction Ground Deformations," *Journal of Soil Dynamics and Earthquake Engineering*, **17**: 427–438.

Taboada VM (1995), "Centrifuge Modeling of Earthquake-induced Lateral Spreading in Sand Using a Laminar Box," *Ph.D Thesis*, Rensselaer Polytechnic Institute, Troy, NY.

Towhata I (2008), "Geotechnical Earthquake

Engineering," *Springer-verlag Berlin Heidelberg*, ISBN 978–3–540–35782–7.

Towhata I, Sasaki Y, Tokida K, Matsumoto H, Tamari Y and Yamada K (1992), "Prediction of Permanent Displacement of Liquefied Ground by Means of Minimum Energy Principle," *Soils and Foundations*, **32**(3): 9–116.

Uzuoka R, Yashima A, Kawakami T and Konard JM (1998), "Fluid Dynamics Based Prediction of Liquefaction induced Lateral Spreading," *Computers and Geotechnics*, **22**(3): 243–282.

Vargas-Monge W (1998), "Ring Shear Tests on Large Deformation of Sand," *Ph.D Thesis*, University of Tokyo.

Vucetic M (1994), "Cyclic Threshold Shear Strains in Soils," *J of GeotechEngng*, ASCE, **120**(12): 2208–2228.

Yasuda S, Nagase H, Kiku H and Uchida Y (1992), "The Mechanism and Simplified Procedure for Theanalysus of Permanent Ground Displacement due to Liquefaction," *Soils and Foundations*, **32**(1): 149–160.

Youd LT, Hansen MC and Bartlett FS (2002), "Revised Multilinear Regression Equations for Prediction of Lateral Spread Displacement," *Journal of Geotechnical and Geoenvironmental Engineering*, **128**(12): 1007–1017.